10

Nitrogen Diffusion in Calcite

Daniele Cherniak, Morgan Schaller, and Bruce Watson

ABSTRACT

Diffusion of N has been measured in natural calcite. For diffusion normal to the {10$\bar{1}$4} cleavage surface, an activation energy for diffusion of 222 ± 17 kJ mol^{-1} and pre-exponential factor of 1.92×10^{-9} m^{2}sec^{-1} are obtained. Diffusion parallel to c is slightly faster than diffusion normal to {10$\bar{1}$4}. These data indicate that N contained in inclusions in calcite will diffuse through the calcite lattice at Earth's upper crustal and surface conditions slowly enough so that calcite may faithfully retain a passive signature of its formation environment for billions of years, providing much needed insight into the cycling of nitrogen between atmosphere, crust, and mantle.

10.1. INTRODUCTION

Nano to microscale mineral inclusions offer a wealth of potential information about the environments of precipitation, and in many cases can be extrapolated broadly to further our understanding large-scale Earth processes such as elemental fluxes and the history of volatile degassing (e.g., see Marty, 2012, for a review). The shallow crustal and atmospheric component of deep nitrogen and carbon cycles is surprisingly not well determined, due in large part to the paucity of minerals that serve as high-fidelity passive recorders of these reservoirs. Calcite-hosted inclusions can contain all of the major atmospheric gases (e.g., Blamey, 2012; Newman et al., 1996; Parry & Blamey, 2010), and are thus a potentially promising source for information on ancient atmospheres. However, the extent to which these records can be quantitatively interpreted depends on the capacity of the host mineral to retain these signatures over geologically relevant timescales. Unlike carbon and oxygen, nitrogen is not an essential constituent of calcite, nor is it a favorable ionic substitution upon crystallization. As such, it is unlikely to be partitioned into the calcite crystal lattice during growth. However, this incompatibility in regular lattice sites does not preclude trapping of N from the aqueous phase during precipitation and subsequent residence within inclusions or occupation of defect sites or interstices of the crystal lattice. Regardless of the mode of incorporation, if the nitrogen in calcite can be extracted and measured, it is vital to understand how retentive the calcite crystal lattice is to nitrogen. This chapter evaluates the kinetics of nitrogen retention by the calcite crystal lattice.

Department of Earth and Environmental Sciences, Rensselaer Polytechnic Institute, Troy, New York, USA

10.2. METHODS

10.2.1. Experimental Procedure

The experiments were performed on natural calcite from Mexico. This material has been used in our previous studies of Sr, Pb, REE, and He diffusion (Cherniak, 1997, 1998; Cherniak et al., 2015). Natural {10$\bar{1}$4} cleavage faces were used in the majority of experiments. To evaluate the potential for diffusional anisotropy, samples were also oriented to investigate diffusion normal and parallel to c.

Specimens were cut into slabs measuring ~2–3 mm on a side and 0.5–1 mm thick for use in individual experiments. The slabs were hand polished to a smooth finish using standard SiC polishing paper, followed by polishing with an automated system in a slurry of 1 μm alumina powder in water, with a final chemical polish using a 0.06 μm colloidal silica suspension.

Carbon in Earth's Interior, Geophysical Monograph 249, First Edition. Edited by Craig E. Manning, Jung-Fu Lin, and Wendy L. Mao.

Nitrogen was introduced into the prepared calcite samples by ion implantation. This approach has been used previously in diffusion studies, including the noble gases He (Cherniak et al., 2009, 2015; Cherniak & Watson, 2011, 2012) and Ne (Cherniak et al., 2014), as well as studies of nitrogen diffusion in other minerals (Watson et al., 2019).

The cut and polished samples were mounted on an aluminum plate with carbon paint and implanted with 100 keV ^{15}N, produced in the Extrion ion implanter at the Ion Beam Laboratory at the University at Albany. Implant doses were 1×10^{15} $^{15}N/cm^2$. ^{15}N was chosen for the ion implants over the more naturally abundant ^{14}N to facilitate analyses with nuclear reaction analysis. The $^{15}N(p, \alpha\ \gamma)^{12}C$ reaction used in these analyses permits greater sensitivity because of the comparatively large cross-section of the reaction. The gamma rays produced in the reaction are also relatively energetic, resulting in fewer interferences with gamma rays that may result from nuclear reactions with other light elements in the samples, as well as those from natural background radiation. After implantation, samples were removed from the aluminum plate and cleaned with ethanol in an ultrasonic bath.

Diffusion anneals of the implanted calcite samples were conducted at near-atmospheric pressure in sealed silica glass ampoules. The implanted samples were placed in silica glass ampoules with a small amount of $CaCO_3$ powder to ensure calcite stability during the diffusion anneals, with silica glass chips to physically separate the samples from the powder; the ampoules were then sealed under vacuum. All experiments were run in Kanthal-wound 1-atm furnaces for times ranging from 2 hours to 7 weeks at temperatures between 600 and 800 °C. Temperatures in furnaces were monitored with chromel-alumel (type K) thermocouples, with temperature uncertainties ~±2 °C.

10.2.2. Nuclear Reaction Analysis (NRA) of Nitrogen

Nitrogen distributions in samples were profiled with NRA using the reaction $^{15}N(p, \alpha\ \gamma)^{12}C$. The strong resonance at 897 keV proton energy was used (e.g. Hirvonen & Lappalainen, 1995; Kumar et al., 2005). The 4.43 MeV gamma rays from the reaction were detected with a high-efficiency bismuth germanate detector. Gamma yield as a function of energy was collected in a multichannel analyzer. Spectra were calibrated using an ^{15}N implanted olivine as a reference sample. Analytical spot sizes for incident proton beams used to induce the reactions are typically 1 mm^2. Beam energies were increased above the resonance energy of the reaction in energy steps of 1 keV in the first few hundred nanometers of depth in the sample, with steps of 5–10 keV at greater depth, to probe ^{15}N distributions at increasing depth in the samples. Depth scales for ^{15}N distributions were determined by the difference between the resonance energy and the incident beam energies, and the energy loss rates for protons in calcite. Energy loss rates were determined through calculations using the SRIM (Stopping and Range of Ions in Matter) software (Ziegler & Biersack, 2006) and standard stoichiometry and density for calcite. During each analytical session, background gamma yields in the energy region of interest were determined by analyzing unimplanted specimens of calcite.

The resultant ^{15}N profiles were fit with a model to determine the diffusion coefficient D. Uncertainties in concentration are primarily a function of counting statistics and backgrounds in the NRA spectra. Uncertainties in depth determination are dominantly a function of the statistical energy spread of individual ions comprising the beam as they travel through the sample (straggle) and the width of the resonance used for the NRA depth profiling, with the former making the largest contribution. Typical depth resolutions are ~10 nm near surface, to a few tens of nanometers several hundred nanometers into the sample (e.g., Cherniak & Lanford, 2001; Hirvonen & Lappalainen, 1995).

Diffusivities were determined using a model with an initial gaussian distribution of diffusant. For a semi-infinite medium with the concentration of diffusant equal to zero at $x = 0$, the distribution of the implanted species can be described as a function of depth x and time t as (Ryssel & Ruge, 1986):

$$N(x,t) = \frac{N_m / 2}{\sqrt{1 + \frac{2Dt}{\Delta R^2}}} \left[\exp\left[-\frac{(x-R)^2}{2\Delta R^2 + 4Dt} \right] \times \left[1 + erf\left[\frac{\frac{R\sqrt{4Dt}}{\sqrt{2}\Delta R} + \frac{x\sqrt{2}\Delta R}{\sqrt{4Dt}}}{\sqrt{2\Delta R^2 + 4Dt}} \right] \right] - \exp\left[-\frac{(x+R)^2}{2\Delta R^2 + 4Dt} \right] \times \left[1 + erf\left[\frac{\frac{R\sqrt{4Dt}}{\sqrt{2}\Delta R} - \frac{x\sqrt{2}\Delta R}{\sqrt{4Dt}}}{\sqrt{2\Delta R^2 + 4Dt}} \right] \right] \right] \quad (10.1)$$

where D is the diffusion coefficient, N_m is the maximum concentration of the implanted species (in an unannealed sample), R is the range (depth in the material) of the implanted species, and ΔR is the range straggle of the initial implanted distribution, which describes the width of the gaussian. Values of R and ΔR for ^{15}N from the Monte-Carlo simulation program SRIM 2006 (Ziegler & Biersack, 2006) are 2370 and 640 Å, and the ^{15}N concentration at the maximum height of the implanted distribution is ~850 ppm for the implant dose of 1×10^{15}/cm^2 for 100 keV ^{15}N in calcite.

Diffusivities were obtained with this model through nonlinear fitting routines to Eq. (10.1) using an approach similar to that outlined in previous work (e.g. Cherniak, 1991; Cherniak et al., 2014; Watson & Dohmen, 2010). Fitting was also done on spectra of implanted, unannealed samples to obtain values for R, ΔR, and N_{imp}, with D determined by fitting the profiles from annealed, implanted samples. The values for R obtained through the fitting procedure of the implanted, unannealed samples were found to agree well with those calculated by the ion implantation simulation program SRIM (Ziegler & Biersack, 2006). The values of ΔR were also found to be consistent with the range straggle predicted by SRIM. In addition to these fitting approaches, simple fits were performed using a gaussian functional form (a broadened gaussian would be the solution to the diffusion equation if the implants were sufficiently deep and/or broadening of the implanted distribution was sufficiently small such that the effects of the surface boundary condition has little influence on N profiles); this approach yielded diffusivities that agreed within uncertainties with those obtained from the other fits. Typical ^{15}N profiles are shown in Figure 10.1.

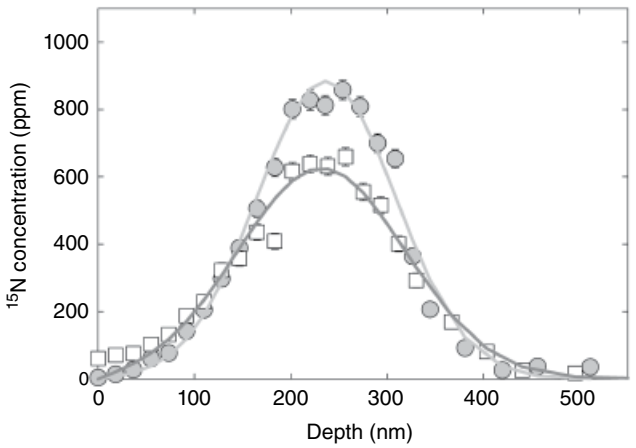

Figure 10.1 Typical ^{15}N profiles in calcite measured by NRA for experiments run at 700 °C for 73 h (grey circles) and 704 °C for 336 h (white squares). See electronic version for color representation of the figures in this book.

10.3. RESULTS

The results from N diffusion experiments on calcite are plotted in Figure 10.2 and presented in Table 10.1. For diffusion normal to {10$\bar{1}$4}, an activation energy of 222 ± 17 kJ/mol and pre-exponential factor of 1.92×10^{-9} m^2/s (log Do = –8.717 ± 0.915) are obtained. There is slight diffusional anisotropy, with diffusion parallel to c faster than diffusion normal to {10$\bar{1}$4}. For this orientation, an activation energy of 218 ± 31 kJ/mol and pre-exponential factor of 4.75×10^{-9} m^2/s (log Do = –8.323 ± 1.634) are obtained. Diffusivities obtained for samples cut parallel to c (for diffusion normal to c) agree within uncertainty with those for diffusion parallel to c.

Results for a time series at 700 °C for diffusion normal to the {10$\bar{1}$4} cleavage surface are plotted in Figure 10.3, illustrating the similarities in diffusivities for anneal times differing by more than a factor of 4, suggesting that what is being measured is volume diffusion of N. The time evolution and conformity of the profiles to the model (Eq. [1]) fit with concentration-independent diffusion coefficients indicate little evidence of concentration-dependence of N diffusion down to concentrations on order of the detection limit for ^{15}N.

10.3.1. O, C, and Noble Gas Diffusion in Carbonates

Diffusivities of other elements in calcite, including C, O, and the noble gases He and Ar, are plotted along with our

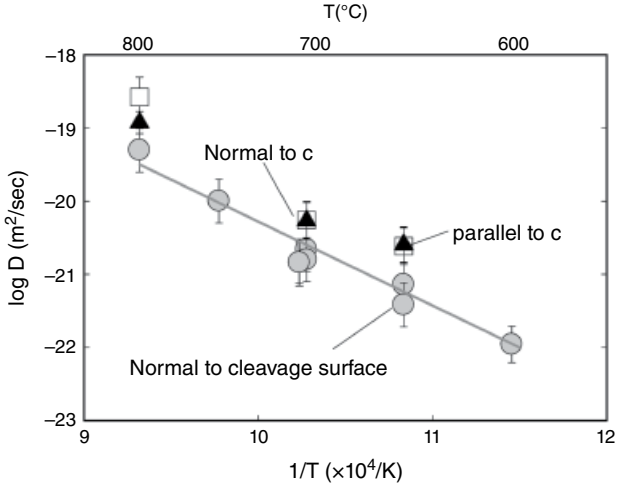

Figure 10.2 Arrhenius plot of N diffusion in calcite. An activation energy of 222 ± 17 kJ/mol and pre-exponential factor of 1.92×10^{-9} m^2/s (log D_o = –8.717 ± 0.915) are obtained from a fit to the data for diffusion normal to {10$\bar{1}$4}. For diffusion parallel to c, we determine an activation energy of 218 ± 31 kJ/mol and pre-exponential factor of 4.75×10^{-9} m^2/s (log D_o = –8.323 ± 1.634). Diffusion normal to c agrees within uncertainty with values for diffusion parallel to c. See electronic version for color representation of the figures in this book.

Table 10.1 N diffusion in calcite.

	T(°C)	time(sec)	D(m^2sec^{-1})	log D	+/–
Diffusion normal to {10$\bar{1}$4}					
NimpCC-12	600	3.79×10^{6}	1.10×10^{-22}	–21.96	0.18
NimpCC-6	650	7.52×10^{5}	7.18×10^{-22}	–21.14	0.10
NimpCC-11	650	1.24×10^{6}	3.82×10^{-22}	–21.42	0.16
NimpCC-2	700	2.63×10^{5}	2.21×10^{-21}	–20.66	0.12
NimpCC-7	700	4.21×10^{5}	2.19×10^{-21}	–20.66	0.11
NimpCC-8	700	6.73×10^{5}	1.64×10^{-21}	–20.79	0.10
NimpCC-13	704	1.21×10^{6}	1.44×10^{-21}	–20.84	0.28
NimpCC-9	750	8.64×10^{4}	9.38×10^{-21}	–20.03	0.11
NimpCC-10	800	7.20×10^{3}	4.96×10^{-20}	–19.30	0.19
Diffusion parallel to c					
NimpCC-19	800	1.08×10^{4}	1.18×10^{-19}	–18.93	0.15
NimpCC-17	700	3.46×10^{5}	5.41×10^{-21}	–20.27	0.25
NimpCC-15	650	7.70×10^{5}	2.56×10^{-21}	–20.59	0.21
Diffusion normal to c					
NimpCC-18	800	1.08×10^{4}	2.64×10^{-19}	–18.58	0.17
NimpCC-16	700	3.46×10^{5}	5.47×10^{-21}	–20.26	0.22
NimpCC-14	650	7.70×10^{5}	2.43×10^{-21}	–20.61	0.27

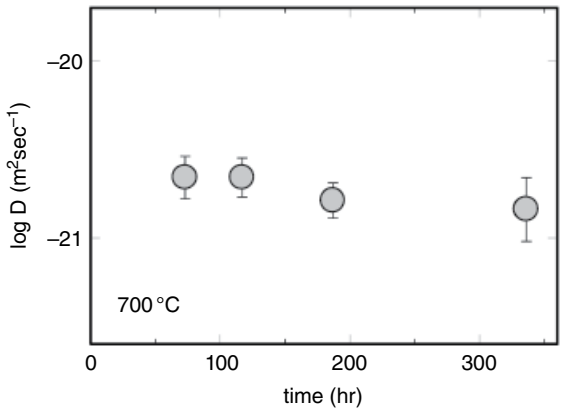

Figure 10.3 Time series for N diffusion in calcite at 700 °C. Similar diffusivities are measured over anneal times differing by up to a factor of 4.6. See electronic version for color representation of the figures in this book.

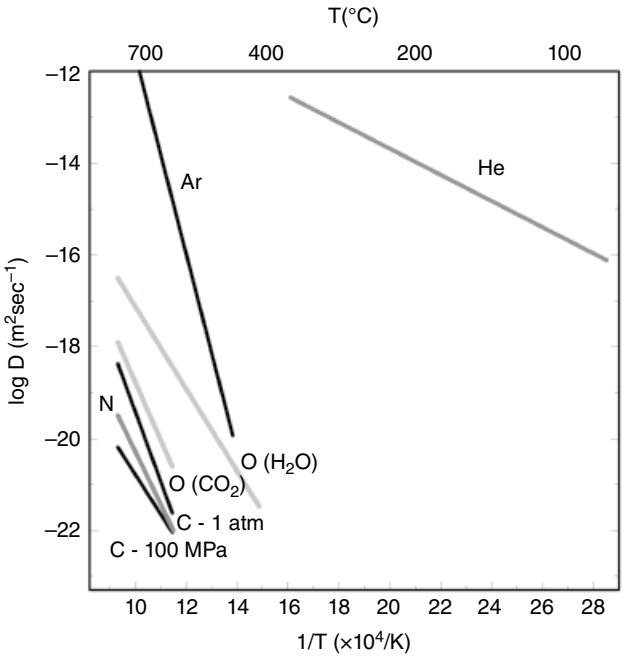

Figure 10.4 Comparison of N diffusion results with C, O, and noble gas diffusion data for calcite. Sources of data: Carbon – Labotka et al. (2000, 2004); Oxygen – Farver (1994), Labotka et al. (2000); He – Cherniak et al. (2015), diffusion normal to {10$\bar{1}$4}; Ar – Cassata and Renne (2013), calculated using an effective diffusion radius of 50 μm. See electronic version for color representation of the figures in this book.

N diffusion data in Figure 10.4. The Arrhenius relation for N diffusion is bracketed by the C diffusion results for 1 atm and 100 MPa (Labotka et al., 2000; Labotka et al., 2004), with the activation energy for N diffusion falling between the values for C diffusion (291 and 166 kJ/mol for 1 atm and 100 MPa, respectively). Diffusion of N is considerably slower than oxygen diffusion, with N diffusing about two orders of magnitude slower than oxygen in a CO_2 atmosphere (Labotka et al., 2000) and three orders of magnitude slower than oxygen in the presence of H_2O (Farver, 1994). We can draw no clear conclusions regarding the mechanism of nitrogen diffusion in the calcite lattice, but recent studies of nitrogen diffusion in silicates (Watson et al., 2019) suggest it may be present in these structures as N_2.

In comparison to the noble gases, N diffuses much more slowly than He and has a much higher activation energy for diffusion (compared with 55 kJ/mol for He in calcite; Cherniak et al., 2015). For example, N will diffuse more than 10 orders of magnitude slower than He at

400 °C, with this variance increasing with decreasing temperature due to the differences in activation energies for diffusion. Ar has a much higher activation energy for diffusion (~420 kJ/mol; Cassata & Renne, 2013) than N, but diffusivities are relatively rapid at higher temperatures; for example, at 400 °C, Ar would diffuse about four orders of magnitude faster than N (with values for Ar diffusivities estimated using the values of D_o/a^2 reported by Cassata and Renne (2013) and an estimated effective diffusion radius a of 50 μm). Because of the differences in activation energies for diffusion of N and Ar, their diffusivities will converge at ~250 °C, and Ar will diffuse more slowly at low temperatures. However, diffusivities at this crossover point are slow (~1×10^{-30} m^2/sec), which would yield diffusion distances of less than 400 nm over times on order of the age of the earth.

10.4. GEOLOGICAL IMPLICATIONS

The results we present here are most relevant to the retention of volatile signatures by calcite over long timescales, regardless of the original mode of incorporation. The fidelity of nitrogen hosted in the interstitial spaces within the crystal lattice (at the molecular scale) or within lattice defects and inclusions (at the nano to micro scale), is important for our interpretation of both low and high temperature calcite fluid inclusion data. The aggregate Arrhenius behavior shown in Figure 10.3 indicates that diffusion of all species (excluding He) from inclusions in calcite is slow enough at Earth's upper crustal and surface conditions that the calcite lattice may be expected to faithfully retain a passive signature of its formation environment for billions of years. This makes calcite a considerable and relatively underexploited source of information on Earth's atmospheric chemistry and volatile degassing history, and may provide much needed information on the cycling of nitrogen between atmosphere, crust, and mantle.

The few tie points we have to constrain the degassing history of the mantle come from N, $\delta^{15}N$, and Ar isotope measurements from chalcedony, chert, and other cryptocrystalline phases (Cadogan, 1977; Marty et al., 2013; Pujol et al., 2013; Sano & Pillinger, 1990). These data are relatively sparse because this information must be gleaned from rare low temperature, upper crustal phases that were originally equilibrated with the atmosphere and have survived the rock cycle at shallow depths of burial. However, fluid inclusions in calcite contain N and Ar (e.g., Newman et al., 1996; Norman et al., 2002; Norman et al., 1996) but have as yet only been treated as a record of local surface or shallow crustal processes, in part due to concerns over the fidelity of calcite as an archive. Our results, when compared to the Ar data of Renne et al. (2009), indicate that if a given sample remains below 250 °C (nominally 8 km of burial) and remains undeformed (Goldstein, 1986, 2001), the diffusive length scale of these species in the lattice will be less than 0.5 μm and the original signature is likely to be retained.

Calcite is omnipresent in surface environments as a primary biogenic and abiogenic precipitate (e.g., skeletal hard parts, speleothems, and soil carbonates, etc.), opening up a new realm of low-temperature archives with a passive record of changes in the concentration of the major atmospheric gases (and their isotope ratios). For example, the ancient atmospheric O_2 and N_2 content may be determined from fluid inclusions in soil carbonates (Schaller et al., 2017; Schaller et al., 2018), and interpretation of these data from ancient samples relies critically on the retention of N by the calcite lattice. Speleothems (Blamey et al., 2016) and biogenic carbonates like brachipod shells (Brand et al., 2016) promise a wealth of information on past gas concentrations, but these results have been treated with a healthy dose of skepticism in part due to doubts about the long-term stability of inclusions in calcite. The evidence presented and compiled here showing the slow diffusion of major atmospheric volatiles in calcite should assuage these concerns.

The calcite archive is potentially very useful in closing the crustal nitrogen cycle. The nitrogen solubility of deep crust and upper mantle minerals has been evaluated (Li & Keppler, 2014; Li et al., 2013), and are important steps in closing the deep crustal nitrogen cycle (Busigny & Bebout, 2013), but we still lack information on N cycling in the shallow crust. Calcite is a common vein-forming mineral from hydrothermal fluids; if volatiles are incorporated into calcite at depth, in the form of veins and other hydrothermal precipitates, will these signatures be retained upon exhumation? To answer this question, we examined several temperature-time path scenarios incorporating the kinetics of N diffusion in calcite. Using a finite-difference computational approach, we allowed nitrogen-bearing calcite crystals of 1 mm radius to cool exponentially from 700 °, 600 °, and 500 °C at three different initial cooling rates (500 °, 100 °, and 10 °C/MYr) and evaluated the fractional loss of nitrogen (F) for each of the nine scenarios. The results of these calculations are shown in Figure 10.5, from which is clear that for any initial temperature below ~500 °C, the loss of nitrogen during exhumation is minimal. For initial temperatures above ~500 °C, N loss can be significant, rising to ~100% for slow cooling at 10 °C/MYr from 700 °C. We emphasize that the curves in Figure 10.4b are not intended to be accurate representations of any natural system but depictions of the general effectiveness of N diffusion in calcite for a range of cooling scenarios. The main shortcomings are the implicit assumptions that (1) N is initially distributed uniformly throughout the calcite crystal and (2) that the crystal remains intact, with no growth, dissolution, or fracturing, during exhumation. These are not realistic assumptions, but the qualitative implications of the

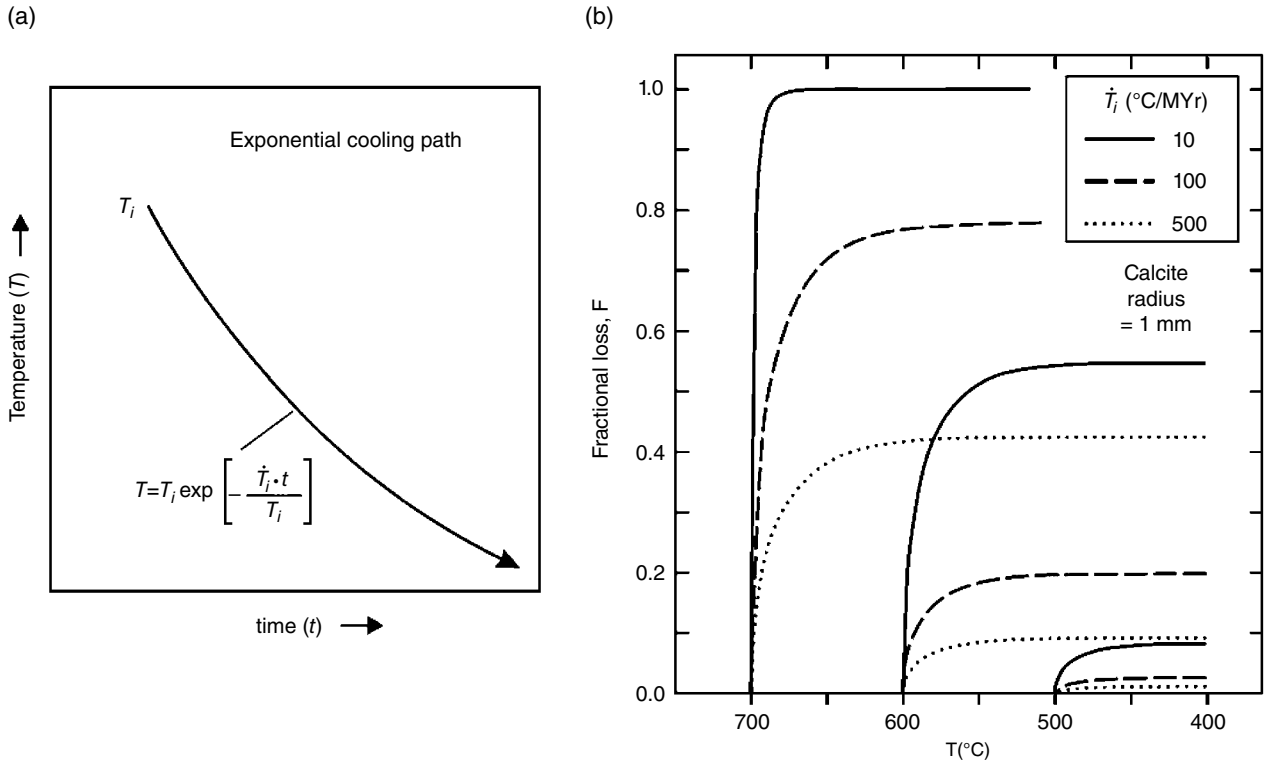

Figure 10.5 (a) Schematic diagram depicting the cooling paths and governing equation used in finite-difference simulations of nitrogen loss from calcite during exhumation and cooling. (b) Model results expressed as fractional N loss (F) vs. temperature for a spherical calcite grain (1 mm radius) cooling from three different initial temperatures (700 °, 600 °, and 500 °C) at three different rates (10 °, 100 °, and 500 °C/Myr). Note the minimal loss resulting from cooling initiated at T < ~500 °C. The results are expressed as fractional loss of N acquired at depth, but the results are equally relevant to fractional gain or isotopic exchange with the surroundings during exhumation. The faster c-parallel diffusion law was used for these calculations. See electronic version for color representation of the figures in this book.

models in terms of calcite retentiveness are nevertheless valid. It should also be borne in mind that the model results apply not only to diffusive loss of N, but also diffusive gain or isotopic exchange. Interestingly, there are some data to suggest a shallow crustal component is retained by calcite following exhumation along faults (Parry & Blamey, 2010), in which case the N_2/CO_2 ratio of calcite inclusions can be used as an indicator of the thermal histories of fluids and to track boiling/condensing processes before inclusion closure (e.g., Norman et al., 2002; Norman et al., 1996).

Busigny et al. (2003) showed that the N flux to the mantle by cool subduction zone processes is highly positively correlated with K content. However, the subducted marine sediments carry with them a substantial load of carbonate minerals, with a potential N content of ~10 ppm. Our results imply that nitrogen incorporated into calcite at the surface or near surface (e.g. from the organic components of marine calcifiers) will be retained long enough to reach a depth where it could become a non-trivial source of N to the lower crust and mantle. Indeed, calcite will survive to a much greater depth in a subduction zone before some amount of it is volatilized and returned to the atmosphere (Kerrick & Connolly, 2001; Tera et al., 1986), compared to sedimentary organic matter that is volatilized at a very shallow depth (see Fischer, 2008, for a review). The volume of this flux is not the focus of the current chapter, but the isotope ratio of this N would be almost certainly atmospheric or biogenic and thus different than the nominal upper mantle or crustal value (see Bebout et al., 2013 for a primer). Though the N in calcite is likely at very low absolute concentrations, the flux of marine biogenic calcite to the mantle is significant over geologic timescales. For a linear heating scenario of 100 °C/MYr, the diffusive opening equations of Watson and Cherniak (2013) reveal that a 2 mm diameter calcite crystal would retain 90% of hosted nitrogen at ~563 °C, 50% at 662 °C, and 10% at 723 °C, i.e., well into the mantle in the cool environment of a subduction zone.

ACKNOWLEDGMENTS

Thanks to Wayne Skala and Hassaram Bahkru for assistance with ion implantation, and to Yuan Li and an anonymous reviewer for their reviews of the manuscript. This work was supported by the Deep Carbon Observatory and the U.S. Department of Energy through grant no. DE-SC0016449.

REFERENCES

Bebout, G. E., Fogel, M. L., & Cartigny, P. (2013). Nitrogen: Highly volatile yet surprisingly compatible. *Elements*, *9*, 333–338.

Blamey, N. J. (2012). Composition and evolution of crustal, geothermal and hydrothermal fluids interpreted using quantitative fluid inclusion gas analysis. *Journal of Geochemical Exploration*, *116*, 17–27.

Blamey, N. J., Boston, P. J., & Rosales-Lagarde, L. (2016). High-resolution signatures of oxygenation and microbiological activity in speleothem fluid inclusions. *International Journal of Speleology*, *45*, 231–241.

Brand, U., Blamey, N., Garbelli, C., Griesshaber, E., Posenato, R., Angiolini, L., et al. (2016). Methane hydrate: Killer cause of Earth's greatest mass extinction. *Palaeoworld*, *25*, 496–507.

Busigny, V., Cartigny, P., Philippot, P., Ader, M., & Javoy, M. (2003). Massive recycling of nitrogen and other fluid-mobile elements (K, Rb, Cs, H) in a cold slab environment: Evidence from HP to UHP oceanic metasediments of the Schistes Lustrés nappe (western Alps, Europe). *Earth and Planetary Science Letters*, *215*, 27–42.

Busigny, V., & Bebout, G. E. (2013). Nitrogen in the silicate Earth: Speciation and isotopic behavior during mineral-fluid interactions. *Elements*, *9*, 353–358.

Cadogan, P. H. (1977). Palaeoatmospheric argon in Rhynie chert. In *Proceedings: Lunar and Planetary Science Conference 1977* (Vol. 8, p. 157).

Cassata, W. S., & Renne, P. (2013). Systematic variations of argon diffusion in feldspars and implications for thermochronometry. *Geochimica et Cosmochimica Acta*, *112*, 251–287.

Cherniak, D. J. (1997). An experimental study of Sr and Pb diffusion in calcite, and implications for carbonate diagenesis and metamorphism. *Geochimica et Cosmochimica Acta*, *61*, 4173–4179.

Cherniak, D.J. (1998). REE diffusion in calcite. *Earth and Planetary Science Letters*, *160*, 273–287.

Cherniak, D. J., Amidon, W., Hobbs, D., &Watson, E. B. (2015). Diffusion of helium in carbonates: Effects of mineral structure and composition. *Geochimica et Cosmochimica Acta*, *165*, 449–465.

Cherniak, D. J., Lanford, W. A. (2001). Nuclear reaction analysis. In Z. Alfassi (Ed.), *Non-destructive Elemental Analysis* (pp. 308–338). Blackwell Science.

Cherniak, D. J., Lanford, W. A., & Ryerson, F. J. (1991). Lead diffusion in apatite and zircon using ion implantation and Rutherford backscattering techniques. *Geochimica et Cosmochimica Acta*, *55*, 1663–1673.

Cherniak, D. J., Thomas, J. B., &Watson, E. B. (2014). Neon diffusion in olivine and quartz. *Chemical Geology*, *371*, 68–82.

Cherniak, D. J., & Watson, E. B. (2011). Helium diffusion in rutile and titanite, and consideration of the origin and implications of diffusional anisotropy. *Chemical Geology*, *288*, 149–161.

Cherniak, D. J., & Watson, E. B. (2012). Helium diffusion in olivine at 1 atm and 2.7 GPa. *Geochimica et Cosmochimica Acta*, *84*, 269–279.

Cherniak, D. J., Watson, E. B., & Thomas, J. B. (2009). He diffusion in zircon and apatite. *Chemical Geology*, *268*, 155–166.

Farver, J. R. (1994). Oxygen self-diffusion in calcite: Dependence on temperature and water fugacity. *Earth and Planetary Science Letters*, *121*, 575–587.

Fischer, T. P. (2008). Fluxes of volatiles (H_2O, CO_2, N_2, Cl, F) from arc volcanoes. *Geochemical Journal*, *42*, 21–38.

Goldstein, R. H. (1986). Reequilibration of fluid inclusions in low-temperature calcium-carbonate cement. *Geology*, *14*, 792–795.

Goldstein, R. H. (2001). Fluid inclusions in sedimentary and diagenetic systems. *Lithos*, *55*, 159–193.

Hirvonen, J. P., & Lappalainen, R. (1995). Nuclear reaction analysis: Particle-gamma reactions. In J. R. Tesmer, M. Nastasi, J. C. Barbour, C. J. Maggiore, & J. W. Mayer (Eds.), *Handbook of modern ion beam materials analysis* (pp. 167–192). Pittsburgh, PA: Materials Research Society.

Kerrick, D., & Connolly, J. (2001). Metamorphic devolatilization of subducted marine sediments and the transport of volatiles into the Earth's mantle. *Nature*, *411*, 293–296.

Kumar, S., Kumar, S. V., Reddy, G.L.N., Kain, V., Ramana, J. V., & Raju V. S. (2005). Depth profiling of nitrogen using 429 keV and 897 keV resonances in the $^{15}N(p,\alpha\gamma)^{12}C$ reaction. *Nuclear Instruments and Methods in Physics Research B*, *240*, 704–710.

Labotka, T. C., Cole, D. R., & Riciputi, L. R. (2000). Diffusion of C and O in calcite at 100 MPa. *American Mineralogist*, *85*, 488–494.

Labotka, T. C., Cole, D. R., Riciputi, L. R., & Fayek, M. (2004). Diffusion of C and O in calcite from 0.1 to 200 MPa. *American Mineralogist*, *89*,799–806.

Li, Y., & Keppler, H. (2014). Nitrogen speciation in mantle and crustal fluids. *Geochimica et Cosmochimica Acta*, *129*, 13–32.

Li, Y., Wiedenbeck, M., Shcheka, S., & Keppler, H. (2013). Nitrogen solubility in upper mantle minerals. *Earth and Planetary Science Letters*, *377*, 311–323.

Marty, B. (2012). The origins and concentrations of water, carbon, nitrogen and noble gases on Earth. *Earth and Planetary Science Letters*, *313–314*, 56–66.

Marty, B., Zimmermann, L., Pujol, M., Burgess, R., & Philippot, P. (2013). Nitrogen isotopic composition and density of the archean atmosphere. *Science*, *342*, 101–104.

Newman, B., Norman, D., Gundimeda, M., & Levy, S. (1996). Understanding the genesis of nonmarine calcite deposits through quadrupole mass spectrometric analysis of fluid inclusion gases. *Chemical Geology*, *132*, 205–213.

Norman, D. I., Blamey, N., & Moore, J. N. (2002). Interpreting geothermal processes and fluid sources from fluid inclusion

organic compounds and CO_2/N_2 ratios. *Proceedings: Twenty-seventh Workshop on Geothermal Reservoir Engineering*, Stanford University, Stanford, California.

Norman, D. I., Moore, J. N., Yonaka, B., & Musgrave, J. (1996). Gaseous species in fluid inclusions: A tracer of fluids and indicator of fluid processes. *Proceedings: Twenty-first Workshop of Geothermal Reservoir Engineering*, Stanford University, Stanford, California.

Parry, W., & Blamey, N. J. (2010). Fault fluid composition from fluid inclusion measurements, Laramide age Uinta thrust fault, Utah. *Chemical Geology*, *278*, 105–119.

Pujol, M., Marty, B., Burgess, R., Turner, G., & Philippot, P. (2013). Argon isotopic composition of Archaean atmosphere probes early Earth geodynamics. *Nature*, *498*, 87–90.

Renne, P. R., Cassata, W. S., & Morgan, L. E. (2009). The isotopic composition of atmospheric argon and $^{40}Ar/^{39}Ar$ geochronology: Time for a change? *Quaternary Geochronology*, *4*, 288–298.

Ryssel, H., & Ruge, I. (1986). *Ion implantation*. New York: John Wiley.

Sano, Y., & Pillinger, C. (1990). Nitrogen isotopes and N_2/Ar ratios in cherts: An attempt to measure time evolution of atmospheric $\delta^{15}N$ value. *Geochemical Journal*, *24*, 315–325.

Schaller, M. F., Pettitt, E., & Knobbe, T. (2017). A potential new proxy for paleo-atmospheric pO_2 from soil carbonate-hosted fluid inclusions applied to pristine Chinle soils from the Petrified Forest 1A core. *Proceedings 2017 AGU Fall Meeting Abstracts*.

Schaller, M. F., Pettitt, E., Knobbe, T., & Breecker, D. (2018). A potential new proxy for paleo-atmospheric pO_2 from soil carbonate-hosted fluid inclusions. *Goldschmidt Conference Abstracts*, *2243*. Boston, MA.

Tera, F., Brown, L., Morris, J., Sacks, I. S., Klein, J., & Middleton, R. (1986). Sediment incorporation in island-arc magmas: Inferences from ^{10}Be. *Geochimica et Cosmochimica Acta*, *50*, 535–550.

Watson, E. B., & Cherniak, D. J. (2013) Simple equations for diffusion in response to heating. *Chemical Geology*, *335*, 93–104.

Watson, E. B., Cherniak, D. J., Drexler, M., Hervig, R. L., & Schaller, M. F. (2019). Nitrogen diffusion in silicate minerals, with implications for nitrogen transport and cycling in the lithosphere. *Chemical Geology*, *516*, 42–58.

Watson, E. B., & Dohmen, R. (2010). Non-traditional and emerging methods for characterizing diffusion in minerals and mineral aggregates. In Y. Zhang & D.J. Cherniak (Eds.), Diffusion in Minerals and Melts, *Reviews in Mineralogy and Geochemistry*, *72*, (pp. 61–105). Chantilly, VA: Mineralogical Society of America.

Ziegler, J. F., & Biersack, J. P. (2006). The stopping and range of ions in matter. *Computer Code SRIM 2006*, http://www.srim.org.